

Impedance computation for power electronic converters with Hilbert transform

Santiago Sanchez*, Gilbert Bergna*, Elisabetta Tedeschi*, Salvatore D'Arco[†], Marina Sanz[‡]

*Norwegian University of Science and Technology - Trondheim, Norway
Email: {santiago.sanchez, gilbert.bergna, elisabetta.tedeschi}@ntnu.no

[†]SINTEF - Trondheim, Norway
Email: salvatore.darco@ntnu.no

[‡]University Carlos III de Madrid - Madrid, Spain
Email: cmsanz@ing.uc3m.es

Abstract

The Hilbert transform (HT) is widely used in signal processing and it has been found as a good tool to understand some physical phenomena in electrical systems. This paper presents a methodology to derive the input impedance of a power electronic converter with the application of the Hilbert transform. The results in the frequency domain based on the Fourier transform are compared with the HT calculations. After an initial example based on a linear circuit, the paper presents the application of the Hilbert transform to calculate the input impedance of a two level power electronics voltage source converter. The results are proved to be in agreement with those obtained from the FFT application. The proposed technique is able to capture the negative resistor behaviour of VSC and an online implementation can be envisioned in the future.

Index Terms

Impedance measurement, nonpassive system, power electronic converters.

I. INTRODUCTION

A common objective from the industry and academia is the future development of more flexible transmission and distribution networks like microgrids, wind farms and multiterminal high voltage direct current networks (HVDC). These grids have the voltage source converter (VSC) topology (e.g. two level, modular multilevel or other configurations) as the main agent acting on the power flow control [1]–[5]. A large number of models for converters and elements of the power electronics based network has been developed in the frequency domain to study the behaviour and the stability of the system with the Nyquist criterium [6]–[10]. Additionally, a major aspect in these stability studies is the modeling and measurements of the power electronic converter input impedance. Some authors have shown by theoretical models that it is possible to observe a negative resistor behaviour embedded in the frequency response of the VSCs e.g. [9], [11]. This negative resistor behaviour is associated with the nonpassivity of the system. In [9] the converter is injecting power into the HVDC grid, and the nonpassive behaviour of the power electronic converter within this HVDC system is shown. Since such behaviour can trigger undesired interactions, its detection through the measurement and elaboration of system values is of significant importance.

In [12], the real time measurement of the impedance is classified as parametric and nonparametric methods. The impedance in the frequency domain is part of the nonparametric approach which does not assume a system model. Furthermore, the computation of the impedances can be subclassified in device impedance and grid impedance. Nowadays, the impedance calculation methods presented in the literature use fast Fourier transform to process the data obtained in the practical experiments [13]. Moreover, some tests use the frequency analyzer devices to obtain the impedance in the frequency domain [14]. Additionally, some estimation techniques, in this case for grid impedance equivalent, have been presented in [15], [16]. Reference [12] stated that the use of sinusoidal current/voltage sweeps to compute the impedance is the most reliable and accurate method and that this is not suited for online measurements due to the measurement time. However, the authors believe that by the application of the HT and use of the characteristics of the discrete form of this transform, it will be possible to reach an online method with a sinusoidal current sweep. The scope of this paper is limited to the validation of the HT for impedance calculation of power electronic converters, leaving the online application for a future publication. The motivation for applying Hilbert transform to the impedance representation described in this paper is based on [17]. The application of the transform has been clearly explained for problems where harmonic analysis is required.

Hence, this paper presents a method to calculate the input impedance of a power electronics converter using the characteristics of the well known Hilbert transform. First, a procedure is carried-out to compute the impedance behaviour in the time domain by the application of the Hilbert transform while the frequency varying disturbance is applied. This test shows that the analysis of the impedance with this methodology reveals the negative resistor behaviour in the VSC. It is remarked

Algorithm 1 Algorithm impedance computation with HT

- 1: **for** $case = 1$ to n **do**
 - 2: Apply the voltage v or current i into the system under test.
 - 3: Store the measurements of i and v .
 - 4: Obtain the HT for the voltage and current $\mathcal{H}(v)$ and $\mathcal{H}(i)$, respectively.
 - 5: Generate the analytic functions $\hat{i} = i + j\tilde{i}$ and $\hat{v} = v + j\tilde{v}$.
 - 6: Calculate the impedance $\hat{z}(t) = \hat{v}(t)/\hat{i}(t) = \mathcal{R}(\hat{z}(t)) + \mathcal{I}(\hat{z}(t))$.
 - 7: Calculate for each point the magnitude of $z(t)$, and angle $\phi(t)$.
 - 8: **end for**
-

that the negative resistor behaviour is observed for the converter under current control. Moreover, the impedance in the frequency domain has been obtained to verify the results obtained with the Hilbert transform procedure. The experimental results have been obtained with a 60 kVA two-level VSC (2L-VSC). An interesting application of the results reached in this paper is their use on the synthesis of an equivalent Norton circuit that can be used in nonlinear stability analysis as the one carried-out in [18]. The paper first presents the basic theory of the Hilbert transform, followed by the explanation of the method used to calculate the impedance with HT and the input impedance measurement of the 2L-VSC from the experimental data. Finally, some conclusions are presented.

II. HILBERT TRANSFORM AND ANALYTIC FUNCTION

The Hilbert transform of a real-valued time-domain signal is another real-valued time-domain signal [19]. The Hilbert transform in this paper will be denoted as $\tilde{x}(t) = \mathcal{H}(x(t))$. One definition uses the convolution integral over the range $-\infty < t < \infty$ and $\tilde{x}(t)$ is defined by

$$\tilde{x}(t) = \int_{-\infty}^{\infty} \frac{x(\tau)}{\pi(t - \tau)} d\tau \quad (1)$$

The transform makes a phase shift operation over sinusoidal signals and keeps its magnitude. Furthermore, the transform shifts $\pi/2$ for positive sequences and $-\pi/2$ for negative sequences [20], therefore the output is orthogonal to the input. Additionally, an analytic function can be described as the real function $f(t)$ plus the imaginary form of its Hilbert transform $\tilde{f}(t)$ as $\hat{x}(t) = f(t) + j\tilde{f}(t) = A(t)e^{j\phi(t)}$, where, the magnitude $A(t)$ varies with time and the instantaneous angular speed value is $\phi'(t) = d(\phi(t))/dt$. Moreover, we can obtain a phase $\phi(t)$ that varies with time. In the paper, $\hat{(\cdot)}$ will be used for analytic functions.

III. METHOD TO CALCULATE THE IMPEDANCE BASED ON THE HT

The strategy to calculate the impedance based on the application of the HT is described in Algorithm 1. A database is required to apply computationally the HT and generate the analytic functions. First it is necessary to define the number of tests (n), the disturbance signal i.e. voltage or current, which is assumed to be known and applied to the system. Followed, the output signal is stored with the disturbance. The next steps are to calculate the HT for the signals and generate the analytic functions for the two signals. The value of the impedance $\hat{z}(t)$ is computed with the analytic functions of the voltage and current \hat{v} and \hat{i} , respectively, as explained in the following subsection.

This section is divided in three examples in order to illustrate the application of the method on the impedance calculation. Subsection III-A presents a theoretic example that introduces the analysis of the impedance based on the HT. The next subsection (III-B) uses a pure sinusoidal input to compute the impedance. Finally, the subsection III-C shows the calculation of an impedance when the input is a chirp signal.

A. Theoretic example

This subsection presents an example of impedance calculation based on the Hilbert transform and the use of analytical functions. To simplify the analysis, the example uses the operator notation $D = d(\cdot)/dt$ for the derivative. The variable $i(t)$ indicates the current through an inductor, L , and a series resistor, R . The voltage across the inductance and the resistance is $u(t)$, such that $u(t) = (LD + R)i(t)$. Using the analytic function it is easy to demonstrate that the voltage is:

$$\hat{u}(t) = (LD + R)\hat{i}(t) = LD\hat{i}(t) + R\hat{i}(t),$$

$$\begin{aligned} \hat{u}(t) &= L(DA_i(t))e^{j\phi_i(t)} + \\ & jLD\phi_i(t)A_i(t)e^{j\phi_i(t)} + RA_i(t)e^{j\phi_i(t)}, \end{aligned}$$

Then, it is possible to define a time varying admittance and impedance of the form:

$$\hat{y}(t) = \frac{\hat{i}(t)}{\hat{u}(t)}, \quad \hat{z}(t) = 1/\hat{y}(t) \quad (2)$$

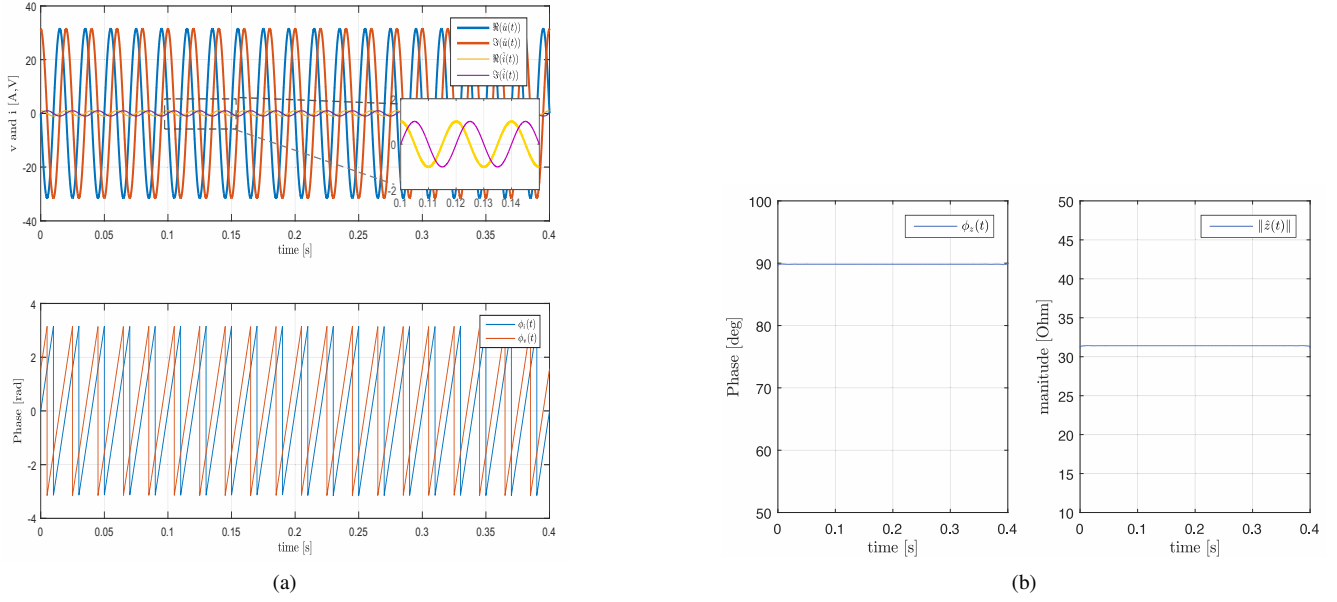


Fig. 1. (a) Voltage and current as analytic functions. Imaginary and real parts of the analytic function for the voltage and current in the time domain (top). Finally, the phase variation for the voltage and current analytic functions (bottom). (b) Impedance with the application of analytic functions, the phase $\phi_z(t)$ in the time domain (left) and the magnitude in the time domain (right).

B. Example of an impedance with the application of the sinusoidal input

This can be exemplified graphically with Fig. 1a by the numerical representation for the case $i(t) = \cos(\omega t)$ which is a stationary signal (Fig. 1a top-left shows the analytic form $\hat{i}(t)$ on the imaginary-real plane). Therefore, the Hilbert transform is $\tilde{i}(t) = \sin(\omega t)$, Fig. 1a shows the voltage across the impedance (top-right), the real and imaginary parts of the analytic function for current and voltage (top) and the phase behaviour for the current and the voltage analytic functions. Besides, the derivatives of the magnitude and the phase are $DA(t) = 0$ and $D\phi(t) = \omega$, respectively. Moreover, the example is reduced to the simple case in which the impedance is constant $\hat{z}(t) = j\omega L + R$, using $\omega = 314.16$ rad/s, $L = 0.1$ H and $R = 0$. The behaviour of the impedance is shown in Fig. 1b. It is clear that the final result is the same as the one obtained with a phasor analysis for a simple inductance and the final value for \hat{z} is as described above.

C. Example of an impedance with the application of a chirp signal as input

A second test is the application of the function chirp for $i(t)$ which is a non-stationary signal (see Fig.2a top and bottom), and it is a frequency swept cosine wave. The waveform is defined by

$$i_{chirp}(t) = \cos(\phi_c(t)) \quad (3)$$

where $\phi_c(t)$ increases or decreases with time. In this case the value for $D\phi(t)$ will change as a function of the time (see the periods of $\phi_v(t)$ and $\phi_i(t)$ changing in Fig. 2a bottom). Mainly, $\|\hat{z}(t)\|$ is increasing as ω increases with the time, and the phase angle of the impedance is changing with ω (Fig. 2b middle and bottom). The tails in Fig. 2b-top for $\hat{z}(t)$ appear due to numerical calculations. The chirp tests are for three values of R , the initial is $R = 0 \Omega$, the second is $R = 2 \Omega$. The third value is $R = -2 \Omega$, which is a signed value that will help in the analysis of nonpassive loads and laboratory test of next section. The literature describes the nonpassive loads as systems with negative resistance behaviour. Moreover, the test shows how the resistor shifts the results in the real axis of the impedance representation. Positive R values produce a positive shift and a negative R moves the impedance to the negative side. An important remark about this result is that a passive energy storage element (e.g. inductance/capacitance) coupled with a non passive element as the negative resistance locates the impedance real part at the negative semi-plane (i.e. real part negative).

IV. IMPEDANCE OF A TWO-LEVEL VOLTAGE SOURCE CONVERTER

A. Experimental setup

The setup is presented in Fig. 3. A 200 kVA voltage source is used to generate the DC voltage (680 V) plus the chirp voltage disturbance superimposed v_{dc} and the current i_{dc} are measured at the terminals of the voltage source, the 60 kVA

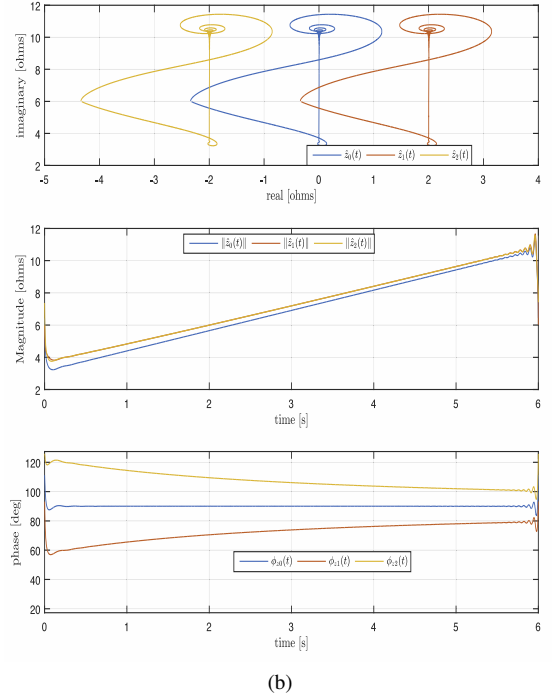
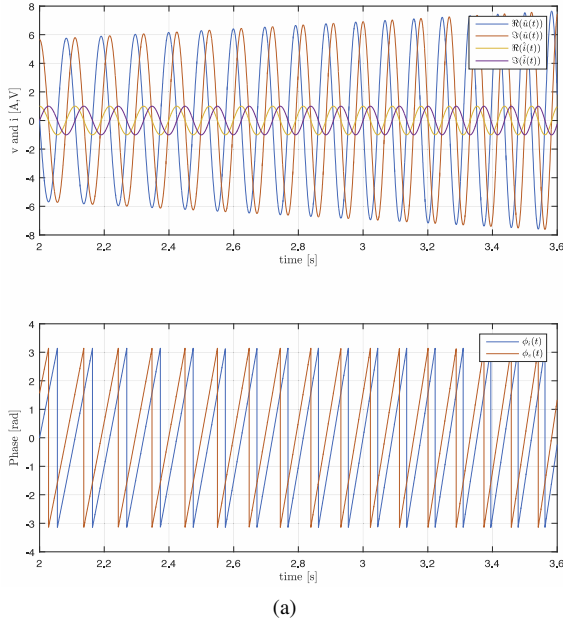


Fig. 2. (a) Voltage and current as analytic functions for the case a chirp cosine is injected. Imaginary and real parts of the analytic function for the voltage and current in the time domain (top). The phase variation for the voltage and current analytic functions (bottom). (b) Impedance with the application of analytic functions. First, impedance in the imaginary-real plane (top), impedance magnitude in the time domain (middle) and the impedance phase $\phi_z(t)$ in the time domain (bottom).

converter i.e. the device under test (DUT) has a capacitor C , an AC LCL filter composed of a converter filter inductor L_f , the filter resistance R_f , the filter capacitance C_f , the grid side filter inductor L_2 , grid side filter resistance R_2 and the three phase IGBTs bridge, the system power flow is controlled with the current controller described in Fig. 3. The controller uses a phase locked loop (PLL) that calculates the electrical angle (θ_{PLL}), the abc signals are transformed to the synchronous reference frame. The current at the abc side is i_{abc} , the voltage is v_{abc} , the output of the current controller is the modulation index at the synchronous reference frame. This modulation index is transformed to abc and finally, it is applied in the converter with a pulse width modulator. The converter parameters are in appendix A. Besides, the laboratory setup is presented in Fig. 4; where a real time simulator OPAL-RT is used to set the voltage of the 200 kVA source and store the data of each test.

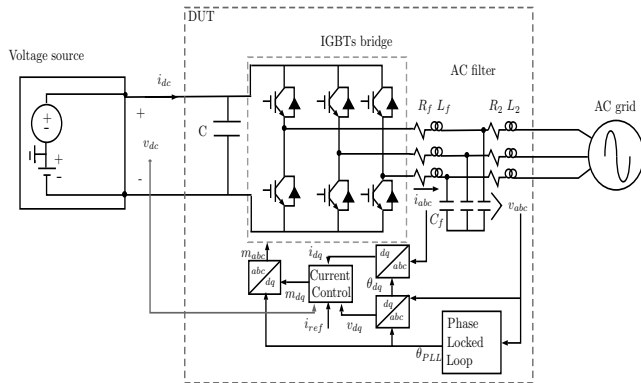


Fig. 3. System setup, device under test DTU, grid emulator and AC grid.

B. Two level voltage source converter

This subsection presents the structure of the controller applied on the two level voltage source converter under test. The control diagram is shown in Fig. 5. The input is the current reference $i_{dq,ref}$, there are feedback variables: the voltage in

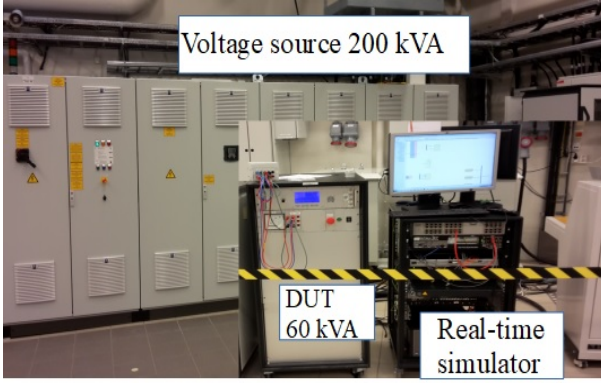


Fig. 4. Laboratory setup, device under test (DTU), voltage source and AC grid.

the synchronous reference frame, the DC voltage term v_{dc} is used to obtain the modulation indices, the current i_{dq} . The controller H_{ci} is a PI and in the Laplace domain is $k_p + k_i/s$. The proportional gain is k_p and the integral gain is k_i .

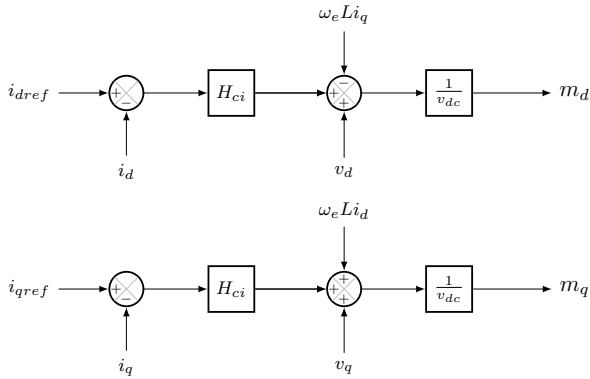


Fig. 5. Current control diagram.

C. Data set and analysis of the results

The input impedance at the DC side of a 60 kVA power electronic voltage source converter at the selected operation point was obtained by the addition of a cosine voltage disturbance. The converter operates consuming constant power from the DC source (injecting the power into the AC network). A data set composed by the voltage and current at the DC side of a 2L-VSC has been obtained, three values of current and two modulation strategies were used to create the data set. The current values at the AC side are 10, 20 and 30 A. The two modulation strategies are compensated modulation and uncompensated modulation [21]. The data uses a sampling frequency of 5 kHz. The signal has been filtered with a bank of discrete FIR filters with order 2^8 , the cut-off frequencies are 0.2×10^{-3} , 0.11 and 0.2 in pu. The filter is designed with the filters toolbox in the Matlab software. Additionally, the disturbance is a voltage with 10 V peak.

Figure 6a shows the 2L-VSC disturbance voltage and current time domain behaviour and the phase variation. In addition, the polar representation of the voltage and current is shown in Fig. 6b. This test uses 10 A at the AC side of the converter. It is important to highlight that the DC components of the signals have been removed. At this stage, the impedance of the 2L-VSC is presented for 10 A in Fig. 7 and Fig. 8a for the three current values. The real part of the impedance is presented in Fig. 7. The magnitude of $\hat{z}(t)$ is shown at the top of Fig. 8a, followed by the phase $\phi_z(t)$ varying with the time. Notice that the impedance has negative real part, which characterizes the nonpassive load behaviour. Furthermore, this negative real part proves the non-passive feature of the system. Finally, to validate the results shown in Fig. 8a, the normal frequency domain test carried-out with the Fourier transform in in Fig. 8b for the same data.

D. Compensated modulation vs uncompensated modulation

Compensated modulation will be used in this paper to refer to the technique consisting in a feedforward *measured* DC voltage signal dividing the controller output to obtain the modulation index. In (4), the modulation index is m , the controller output is $y_o(t)$ and the measured dc voltage is $v_{dc}(t)$. However, for the converter used this voltage is filtered by a low pass

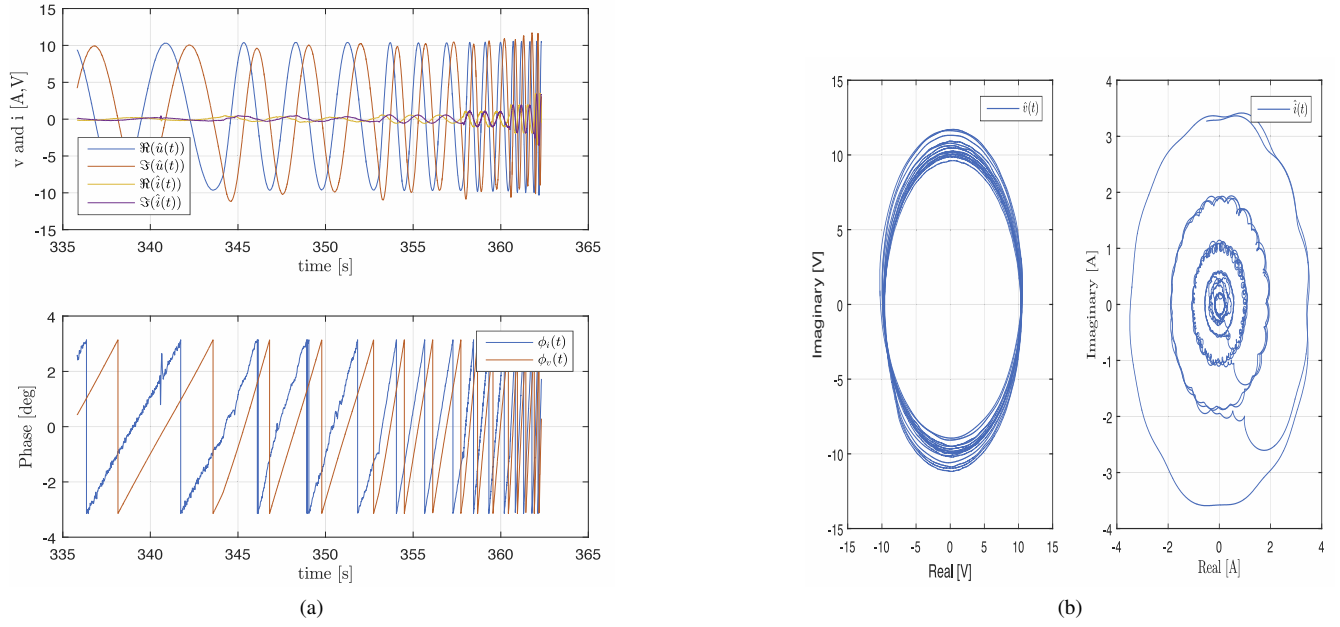


Fig. 6. (a) Current and voltage (top) at the DC side of the 2LVSC as analytic functions, phase of current and voltage. Case 10 A at AC side of the converter. (b) Voltage and current for the 2L-VSC. Imaginary and real parts of the analytic function for the voltage and current polar form.

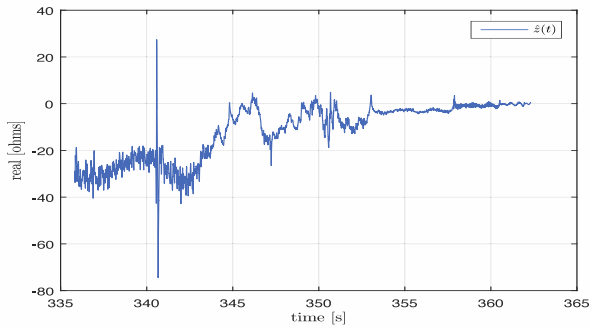


Fig. 7. Real part of the impedance for the case the AC current is controlled to 10 A.

filter described at the appendix. The uncompensated modulation (5) uses a constant value dividing the controller output and does not have a feedforward of the voltage. In (5) the modulation index is m , the controller output is $y_o(t)$ and a constant DC voltage value is V_{dc} .

$$m = \frac{y_o(t)}{v_{dc}(t)} \quad (4)$$

$$m = \frac{y_o(t)}{V_{dc}} \quad (5)$$

The objective of this test is to observe any possible change on the impedance behaviour of the converter due to the modulation strategies. According to Fig. 9, the converter presents similar behaviour for the both types of control strategies with AC current of 10 A. Figure 9 shows the nonpassive system behaviour where the angle at low frequencies is lower than -90 degrees for both cases. The results do not show the effects of the controller and highlight the nonpassive behaviour with a capacitor in parallel i.e. the C of the converter. The comparison between the two modulation strategies is reported in the appendix B for the Fourier transform.

V. CONCLUSIONS

The Hilbert transform is a useful signal processing tool which can be used on the time domain for the estimation of converter input impedances. The results show the impedance with a negative resistance that is not easily observed on the frequency domain (where the angle is used to understand this result). This reveals a drawback with the pure frequency domain impedance representation. However, with analytic functions the negative or positive resistor is calculated in one

step. The passivity of the frequency domain impedance representation has been described in the literature as the real part with positive values [22], which refers to the angle of a linear passive system between -90 and $+90$ degrees and it has been shown in the test above how the converter crosses the limit. Moreover, the non-linear theory based on dissipation defines a passive element e.g. one element with positive resistance, and the test for the converter shows the negative real part of the impedance (i.e. the negative resistance).

One of the characteristics of the method presented in this paper is that it is possible to get information similar to the one obtained by a time-frequency transform. In this case we have the frequency as an input for the disturbance plus the magnitude/phase of the impedance in the time domain. Moreover, some of the samples can present problems of noise and sensors measurements. Therefore, one of the applications of this methodology is to use time information of the signals to calculate the impedance and see how a notch or spike in the signal can produce computation errors.

Future research will be focused on the *online* application of the method. The discrete form of the HT can be applied on this type of test. Since, the DC impedance uses one current and one voltage, a common discrete HT filter can be applied to both signals and the properties of them are kept.

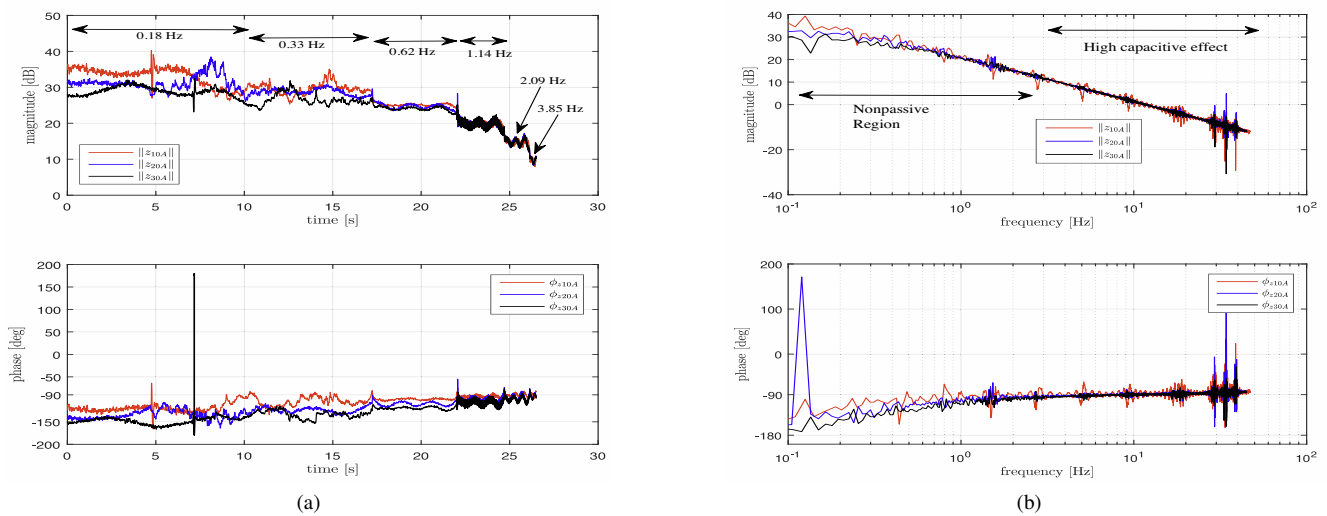


Fig. 8. (a) Impedance with the application of analytic functions. Impedance magnitude in the time domain (top) and the impedance phase $\phi_z(t)$ in the time domain (bottom). (b) Impedance with Fourier analysis. Impedance magnitude in the time domain (top) and impedance phase ϕ_z (bottom).

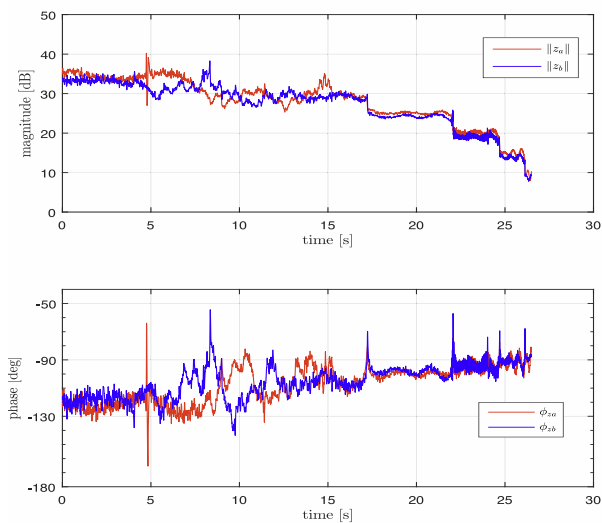


Fig. 9. Comparison of the control strategies, compensated and uncompensated modulations for 10A current at the AC side of the converter. Compensated modulation (Z_a , red) and uncompensated modulation (Z_b , blue).

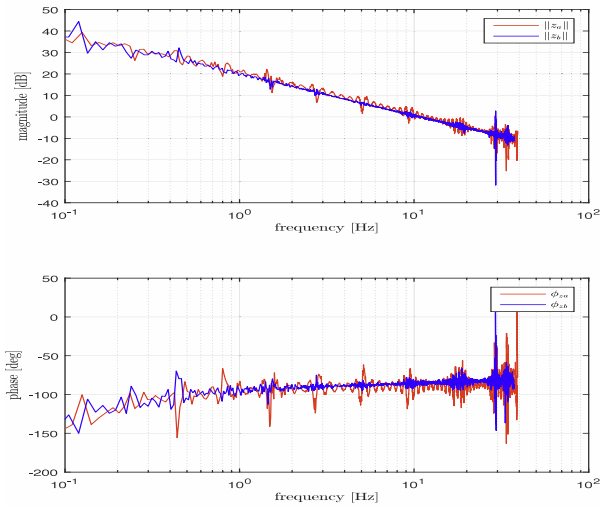


Fig. 10. Comparison of the control strategies, compensated and uncompensated modulations for 10A current at the AC side of the converter. Compensated modulation (Z_a , red) and uncompensated modulation (Z_b , blue).

VI. ACKNOWLEDGMENT

This project has received funding in the framework of the joint programming initiative ERA-Net Smart Grids Plus, with support from the European Union’s Horizon 2020 research and innovation programme and Research council of Norway.

APPENDIX

A. Two level converter parameters

The converter has the following parameters: rated apparent power 60 kVA, the rated voltage is 400 V, the rated frequency is 50 Hz, the switching frequency is 5 kHz, the DC capacitor is 14.1 μF , the AC filter inductor is $L_f=0.5$ mH, the filter resistor is $R_f = 32$ m Ω , the filter AC capacitor is $C_f = 50$ μF , the grid side filter is $L_2 = 0.5$ mH and $R_2 = 32$ m Ω . The IGBTs three-phase bridge is a SEMIKUBE -size 1, it has embedded the capacitor C . The controller proportional gain is $k_p = 0.5$ pu, the integral gain is $k_i = 65$ pu. The DC voltage measurement filter has a discrete form $(10z + 10)/(11z + 9)$ with sampling frequency $F_s = 5$ kHz.

B. Impedance in the frequency domain

The impedance in the frequency domain is presented in Fig. 10 to demonstrate the correct behaviour of the application of the HT on the data set.

REFERENCES

- [1] W. G. B4.57, *Guide for the Development of Models for the HVDC Converters in a HVDC Grid*. CIGRE, 2014.
- [2] M. Amin and M. Molinas, “Understanding the origin of oscillatory phenomena observed between wind farms and hvdc systems,” *IEEE Journal of Emerging and Selected Topics in Power Electronics*, vol. 5, no. 1, pp. 378–392, March 2017.
- [3] J. Freytes, S. Akkari, J. Dai, F. Gruson, P. Rault, and X. Guillaud, “Small-signal state-space modeling of an hvdc link with modular multilevel converters,” in *2016 IEEE 17th Workshop on Control and Modeling for Power Electronics (COMPEL)*, June 2016, pp. 1–8.
- [4] S. Sanchez and M. Molinas, “Degree of influence of system states transition on the stability of a dc microgrid,” *Smart Grid, IEEE Transactions on*, vol. 5, no. 5, pp. 2535–2542, Sept 2014.
- [5] G. P. Adam, S. J. Finney, and B. Williams, “Interoperability of voltage source converters in dc grids,” *IET Generation, Transmission Distribution*, vol. 7, no. 11, pp. 1310–1317, November 2013.
- [6] J. Sun, “Impedance-based stability criterion for grid-connected inverters,” *Power Electronics, IEEE Transactions on*, vol. 26, no. 11, Nov 2011.
- [7] —, “Small-signal methods for ac distributed power systems—a review,” *IEEE Transactions on Power Electronics*, vol. 4, no. 11, pp. 2545–2554, Nov. 2009.
- [8] H. Liu and J. Sun, “Impedance-based stability analysis of vsc-based hvdc systems,” in *2013 IEEE 14th Workshop on Control and Modeling for Power Electronics (COMPEL)*, June 2013, pp. 1–8.
- [9] G. Pinares and M. Bongiorno, “Analysis and mitigation of instabilities originated from dc-side resonances in vsc-hvdc systems,” *IEEE Transactions on Industry Applications*, vol. 52, no. 4, pp. 2807–2815, July 2016.
- [10] M. Amin and M. Molinas, “Impedance based stability analysis of vsc-based hvdc system,” in *2015 IEEE Eindhoven PowerTech*, June 2015, pp. 1–6.
- [11] G. Pinares and M. Bongiorno, “Modeling and analysis of vsc-based hvdc systems for dc network stability studies,” *IEEE Transactions on Power Delivery*, vol. 31, no. 2, pp. 848–856, April 2016.
- [12] T. Roinila, M. Vilkkö, and J. Sun, “Online grid impedance measurement using discrete-interval binary sequence injection,” in *2013 IEEE 14th Workshop on Control and Modeling for Power Electronics (COMPEL)*, June 2013, pp. 1–8.
- [13] J. Huang, K. A. Corzine, and M. Belkhaty, “Small-signal impedance measurement of power-electronics-based ac power systems using line-to-line current injection,” *IEEE Transactions on Power Electronics*, vol. 24, no. 2, pp. 445–455, Feb 2009.

- [14] X. Chen and J. Sun, "A study of renewable energy system harmonic resonance based on a dg test-bed," in *2011 Twenty-Sixth Annual IEEE Applied Power Electronics Conference and Exposition (APEC)*, March 2011, pp. 995–1002.
- [15] H. Gu, X. Guo, D. Wang, and W. Wu, "Real-time grid impedance estimation technique for grid-connected power converters," in *2012 IEEE International Symposium on Industrial Electronics*, May 2012, pp. 1621–1626.
- [16] W. Ghzaiel, M. J. B. Ghorbal, I. Slama-Belkhdja, and J. M. Guerrero, "A novel grid impedance estimation technique based on adaptive virtual resistance control loop applied to distributed generation inverters," in *2013 15th European Conference on Power Electronics and Applications (EPE)*, Sept 2013, pp. 1–10.
- [17] D. Jeltsema, "Budeanu's concept of reactive and distortion power revisited," in *2015 International School on Nonsinusoidal Currents and Compensation (ISNCC)*, June 2015, pp. 1–6.
- [18] A. Griffio and J. Wang, "Large signal stability analysis of 'more electric' aircraft power systems with constant power loads," *IEEE Transactions on Aerospace and Electronic Systems*, vol. 48, no. 1, pp. 477–489, Jan 2012.
- [19] J.-S. Bendat and A.-G. Piersol, *Random Data, Analysis and measurement procedures*. Wiley, 2010.
- [20] J. S. Bendat and A. G. Piersol, *Random Data, analysis and measurements procedures*, 4th ed. WILEY, 2010.
- [21] G. Bergna-Diaz, J. A. Suul, and S. D'Arco, "Small-signal state-space modeling of modular multilevel converters for system stability analysis," in *2015 IEEE Energy Conversion Congress and Exposition (ECCE)*, Sept 2015, pp. 5822–5829.
- [22] P. Moylan, *Dissipative Systems and Stability*. www.pmoylan.org, 2014.